Collective Expansion in High-Energy Nuclear Collisions – The search for the partonic EOS at RHIC

Nu Xu
Nuclear Science Division
Lawrence Berkeley National Laboratory, Berkeley, CA 94720, USA

We discuss recent results from RHIC. Issues of energy loss and partonic collectivity from $Au + Au$ collisions at $\sqrt{s_{\rm NN}} = 200$ GeV are the focus of this paper. We propose a path toward the understanding of the partonic Equation of State in high energy nuclear collisions.

1. Introduction

The purpose of the heavy ion program at Brookhaven National Laboratory is to probe strongly interacting matter under extreme conditions, *i.e.* at high densities and temperatures. Naturally the search for the existence of a new form of matter - the quark-gluon plasma (QGP) - is the experimental focus of the program.

Lattice QCD calculations [1,2] predict a transition or fast cross-over between QGP and the hadronic state at $T_c \approx 150 - 180$ MeV with vanishing baryon density. Including finite baryon density does not affect the general properties of the transition in Lattice QCD [3]. The energy density at the transition point is determined to be $\epsilon_c \approx 0.7 - 1.0$ GeV/fm^3. Under the same condition, chiral symmetry restoration also happens [1]. Therefore experimentally one would search for signatures of both QGP formation and in-medium effects of hadron properties.

In high-energy nuclear collisions, the term flow has two important aspects: (i) collectivity of produced hadrons and (ii) the local thermalization among these hadrons [4]. As long as there are interactions among constituents, collectivity of the matter will be developed provided that the distribution of matter density is inhomogeneity. When the interactions last long enough the system will approach local equilibrium and hence develops hydrodynamic type flow. At the early stage of high-energy nuclear collision, both the matter density and its gradient are large, therefore we expect the development of partonic collectivity - the collective motion of partons. The issues of thermalization can be addressed by studying heavy-flavor ($c-, b-$ quarks) collectivity, because the collisions that generate the collective motion for heavy-quarks will likely lead to thermalization among the light quarks ($u-, d-, s-$ quarks). It is important to note that collectivity is cumulative through the expansion phase and is not affected by the details of the hadronization process.

Many exciting results have merged from the RHIC experiments since they first started in the year 2000. Using high transverse momentum hadrons we have demonstrated interactions at the early stage of the collisions. These experimental effects are most likely

caused by the interactions among the partons. Much stronger collective flow has been observed, especially for the early developing v_2, compared to results from lower energy heavy ion collisions. This implies that the intensive rescattering effects arise from the partonic stage at RHIC.

This report will summarize the recent results from experiments at RHIC. It will be divided into three parts: (i) observations at the intermediate transverse momentum region ($3 \leq p_T \leq 10$ GeV/c); (ii) bulk properties of the matter produced at RHIC; (iii) evidence of partonic collectivity at RHIC. Finally, the report will be ended with a brief summary and outlook.

2. Energy loss – Interactions at early partonic stage

The measurements of hadron yields at intermediate transverse momentum region ($3 \leq p_T \leq 10$ GeV/c) have demonstrated that hot and dense matter is produced in $Au + Au$ collisions at RHIC [5–7]. Nuclear effects on the inclusive spectra are measured by comparison to a nucleon-nucleon (NN) reference via the nuclear modification factor[1]

$$R_{AB}(p_T) = \frac{d^2N^{AB}/dp_T d\eta}{T_{AB} d^2\sigma^{pp}/dp_T d\eta} \tag{1}$$

where $T_{AB} = \langle N_{bin} \rangle / \sigma_{inel}^{NN}$ from a Glauber calculation accounts for the nuclear collision geometry. The spectrum of non-single-diffractive (NSD) $p + p$ interactions was used. Figure 1 shows $R_{AA}(p_T)$ at $\sqrt{s_{\rm NN}} = 200$ GeV for centrality selected $Au + Au$ spectra relative to the measured $p + p$ spectrum. Horizontal hatched bands show expectations (estimated from Glaubal model calculations) for scaling of the yield with $\langle N_{bin} \rangle$ (right side, lightly shaded) or mean number of participants $\langle N_{part} \rangle$ (left side, darkly shaded) and the widths showing their respective uncertainties. It is evident that hadron production for $6 \leq p_T \leq 10$ GeV/c is suppressed by a factor 4-5 in central $Au + Au$ collisions relative to $p + p$ collisions. The apparent suppression decreases monotonically from central to peripheral $Au + Au$ collisions. Compared with $p + p$ collisions, the spectrum from central $Au + Au$ collisions is modified, presumably due to rescatterings of energetic particles in the hot and dense medium.

[1]The nuclear modification factor can also be extracted from the ratio of R_{CP} (ratios of central over peripheral collisions):

$$R_{CP}(p_T) = \frac{[dN/(N_{bin} dp_T]^{Central}}{[dN/(N_{bin} dp_T]^{Peripheral}}$$

where $R_{CP} \sim 1$ if particle production is equivalent to a superposition of independent nucleon-nucleon collisions. Except the nuclear collision geometry, both R_{CP} and R_{AB} represent the same physics.

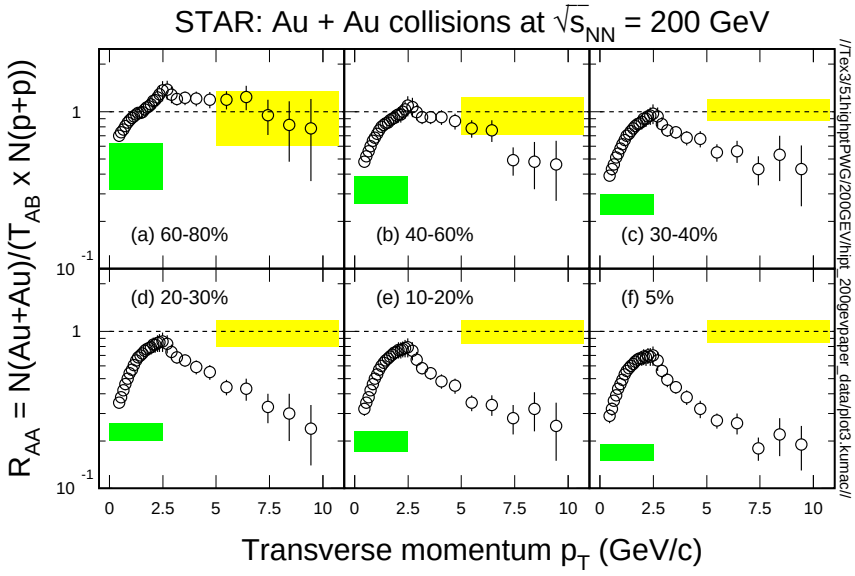

Figure 1 *Mid-rapidity charged hadron $R_{AA}(p_T)$ in ($|\eta| \leq 0.5$), for centrality selected $Au+Au$ spectra relative to the measured $p+p$ spectrum. The $p+p$ spectrum is common to all panels. The left hatched bands denote the uncertainties in determining the number of participants, the right hatched bands indicate the uncertainties in determining the number of binary collisions.*

Note that the basic idea behind the nuclear modification factor R_{AB} is to normalize the transverse momentum distribution from nuclear collisions to that from elementary $p+p$ collisions [8,9]. The normalization is done with the assumption of binary collision $\langle N_{bin} \rangle$ scaling in hard collisions:

$$\sigma_{pA} = \sigma_{NN} \times A^{\alpha}, \tag{2}$$

with $\alpha = 1$. However, up to $p_T \sim 10$ GeV/c, the scaling is violated in hadron productions in all $p + A$ collisions [10,11]. The exceptions are Drell-Yan processes and direct photon production [10,12]. This indicates that the observed p_T broadening effect in proton induced interactions is, at least partly, in my view, due to final state interactions, *i.e.*, the interaction among the produced particles. Since heavy flavors are created at the early stage of the collision, a comparison of the R_{AB} results from both $Au + Au$ and $d + Au$ collisions will shed light on this problem.

When normalized to the corresponding number of binary collisions, the hadron productions at intermediate p_T in ultra-relativistic interactions of heavy nuclei reveal a clear suppression of both the single-particle inclusive yields [5,6,13–15] and back-to-back pairs [16,17] in the most central $Au+Au$ collisions (5%) (see Figures 1 and 2). There are three possible explanations:

1. **Initial Condition:** In this hypothesis, the suppression results from initial-state effects prior to the hard scattering, such as the saturation of gluon density in the incoming nuclei [18]. Subsequent interactions merely materialize the hadrons from the intrinsic parton distributions.

2. **Parton Energy Loss:** Energetic partons created via hard scatterings traverse the hot and dense medium and lose their energy. The observed highly correlated high p_T hadrons are primarily those created from partons produced near the surface and directed outwards. In this scenario, the interactions take place at the parton stage and the effect is called "jet-quenching" [19].

3. **Hadron Energy Loss:** Qualitatively, due to scatterings among hadrons, the fragmented hadrons should also suffer energy loss, as discussed in Ref. [20]. An energetic parton often leads to a cluster of highly correlated hadrons; therefore, one might expect a different pattern in the suppression and azimuthal distributions between partonic and hadronic energy loss.

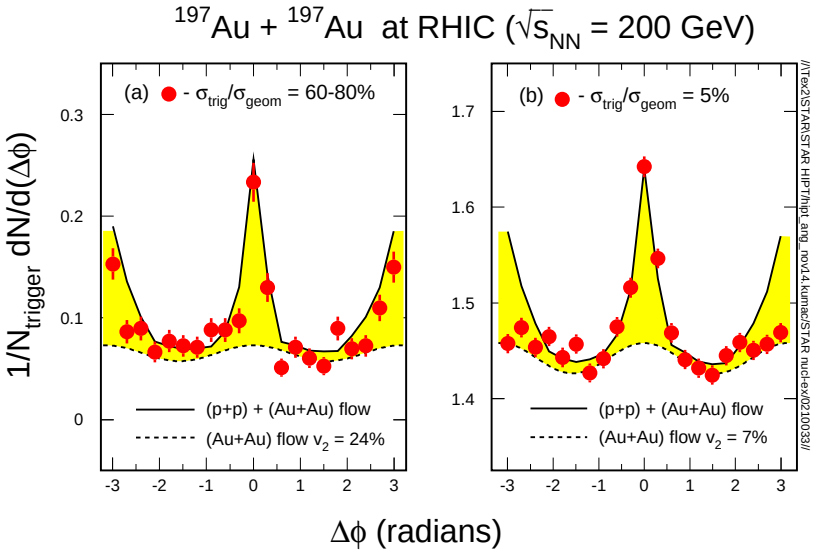

Figure 2 *Mid-rapidity azimuthal distributions from peripheral (left-plot) and central (right-plot) Au + Au collisions at 200 GeV. The dashed-lines represent the anisotropy distributions (often called elliptic flow) from low p_T hadrons at corresponding collision centrality. The solid-lines are the sum of the azimuthal distributions from p + p and flow. The back-to-back hadrons are clearly suppressed in central collisions.*

In order to discriminate between initial condition and final state interaction induced parton energy loss, a study of $d + Au$ collisions was performed. The STAR results [7] are sketched in Figure 3: Left: R_{AB} for central $d + Au$ (20%) and central $Au + Au$ (5%) collisions at $\sqrt{s_{\rm NN}} = 200$ GeV; Right: Comparison of two-particle azimuthal distributions for central $d + Au$ (20%) collisions to the minimum bias $p + p$ and central $Au + Au$ (5%) collisions.

The nuclear modification factor R_{AB} clearly shows the dramatic difference between central $d+Au$ and $Au+Au$ collisions and the same is true for the azimuthal distributions. In fact, the azimuthal distributions in $d+Au$ collisions are similar to those of $p+p$ collisions. The R_{AB} results from all RHIC experiments are consistent [21–23].

The fact that no suppression in hadron yields from $d + Au$ collisions for $2 \leq p_T \leq 7$ GeV/c is seen and the two-particle azimuthal distribution in $p + p$ and $d + Au$ collisions are similar suggests that the suppression observed in central $Au + Au$ collisions is due to final-state interactions. Here the term final-state interaction refers to the reactions

among the produced particles, either partons with partons or hadrons with hadrons, or both. It remains an open issue whether partonic or hadronic interactions dominate such processes that lead to the observed suppression at RHIC. However, during the early stage of high-energy nuclear collisions both particle density and energy density are high, and the wave-functions of particles are overlapping. One might wonder whether the concept of hadronic interactions at such stage is meaningful.

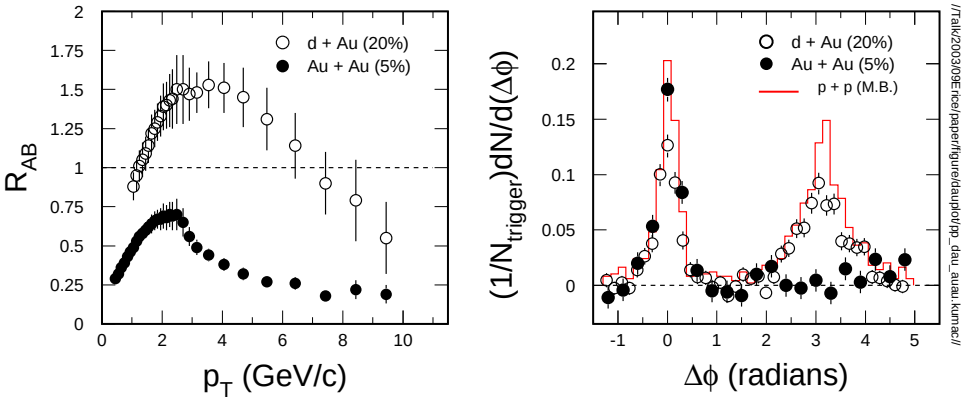

Figure 3 Left: *R_{AB} for central $d+Au$ (20%) and central $Au+Au$ (5%) collisions at $\sqrt{s_{\rm NN}}$ = 200 GeV;* **Right:** *Comparison of two-particle azimuthal distributions for central $d+Au$ (20%) collisions to the minimum bias $p+p$ and central $Au+Au$ (5%) collisions.*

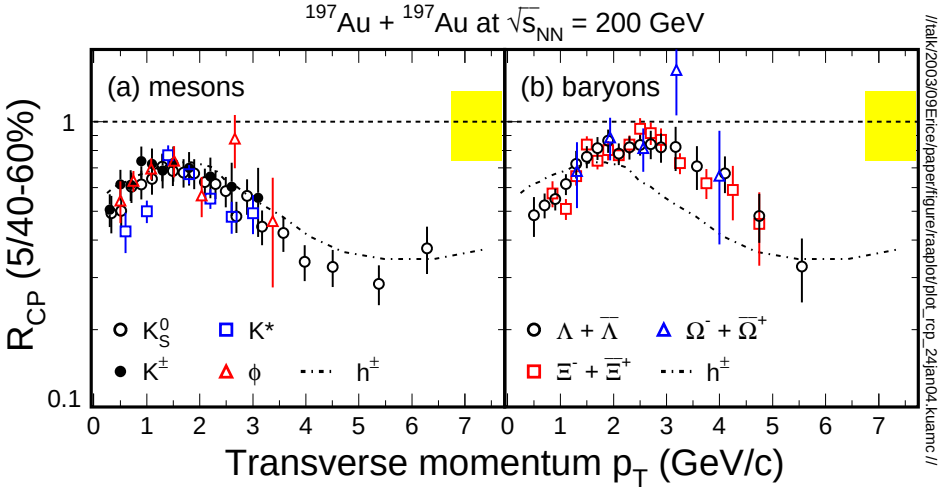

Figure 4 *STAR preliminary results of mid-rapidity R_{CP}, 0-5% over 40-60%, for mesons (a) and baryons (b). The R_{CP} of charged hadrons is also shown as dot-dashed lines in both plots. The error bars shown include both statistical and systematic errors. The widths of the gray band represent the uncertainties in model calculations of N_{bin}, the number of binary collisions.*

Figure 4 shows the STAR preliminary results [24–26] of mid-rapidity R_{CP} for mesons (a) and baryons (b), using the top 5% central collisions normalized by the 40-60% peripheral

collisions. For the p_T region $2 \leq p_T \leq 4$ GeV/c, R_{CP} for baryons is similar to expectations of N_{bin} scaling and $R_{CP}^{meson} \leq R_{CP}^{baryon}$. At higher p_T ($p_T \geq 5$ GeV/c), the values of R_{CP} begin to decrease and merge together with that of charged hadrons.

The particle type dependence of R_{CP} at intermediate p_T is in contradiction with the expectations from energy loss followed by fragmentation in vacuum. The enhancement of yield at intermediate p_T in proton induced collisions, *i.e.* the Cronin effect [27], has been observed at all collision energies with a larger effect of the enhancement for protons than for mesons [28]. The Cronin effect has been attributed to initial-state rescattering. The strong particle-type dependence of the effect indicates a medium modification to the parton fragmentation: the final hadron spectrum is affected by both the type of the hadron and the medium. In $p+p$ or $p+A$ collision, parton fragmentation dominates the hadronization process. The suppression and the particle-type dependence of R_{CP} (see Figure 4) may reflect bulk partonic matter hadronization in heavy ion collisions.

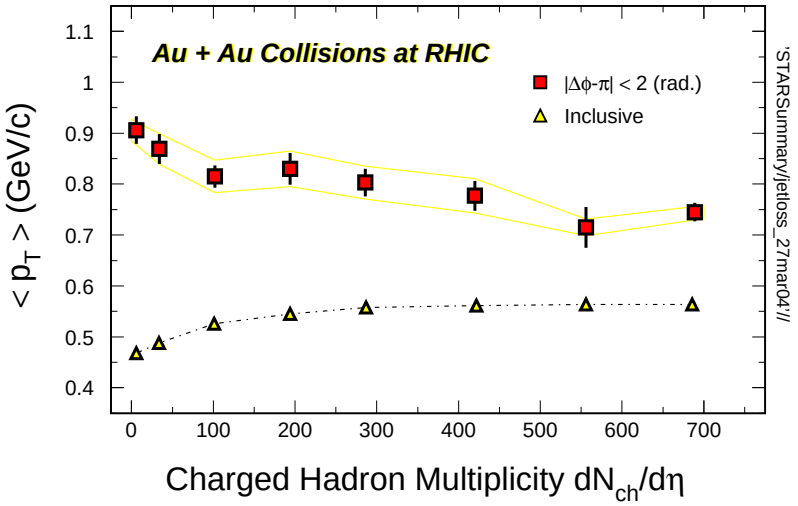

Figure 5 *STAR preliminary results of centrality dependence of the associated charged hadron $\langle p_t \rangle$ from the away-side in 200 GeV $p+p$ (leftmost point) and $Au+Au$ collisions (squares). In each case, opposite a trigger hadron with p_T in the 4-6 GeV/c range. The upper and lower lines represent the systematic uncertainties in $Au+Au$ collisions. The values of $\langle p_t \rangle$ for inclusive hadron production is shown as triangles and dashed line.*

It is obvious that the description of the energy loss of a jet or a fast moving hadron in the hot and dense medium is only possible from a microscopic point of view. The energetic object (parton or hadron) is viewed as a microscopic probe. Indeed, pQCD inspired model calculations are all constructed with this concept [19,29]. The approaches based on coherence effects [18] appear not to work, at least for results at mid-rapidity at RHIC. However, because the system created in $Au+Au$ collisions is large, hot and dense, collective motion at the macroscopic level must exist. In the following sections, we will discuss collective behavior observed in high-energy nuclear collisions.

The centrality dependence of $\langle p_t \rangle$ of the associated away-side charged hadrons in comparison to that of the inclusive hadron production in 200 GeV $Au+Au$ collisions is shown in Figure 5. While in peripheral collisions, the values of $\langle p_t \rangle$ for the away-side hadrons are significantly larger than that of inclusive hadrons, the two values approach each other

with increasing centrality [30]. Within the argument of 'jet quenching', the results suggest that even a moderately hard parton traversing a significant path length through the hot and dense medium makes substantial progress toward equilibration with the bulk matter. Therefore the rapid attenuation of the parton energy (see Figure 3) and the attainment of thermalization via parton interactions in the earliest collision stages would become possible in $Au+Au$ collisions at RHIC. The results from Ref. [30] indeed make the connection between local partonic interaction properties and global characteristics of thermalization.

3. Hadron spectra – Bulk properties

In this section, we will discuss the transverse momentum spectra of identified hadrons with the focus on proton, ϕ, multi-strange baryons and their freeze-out properties.

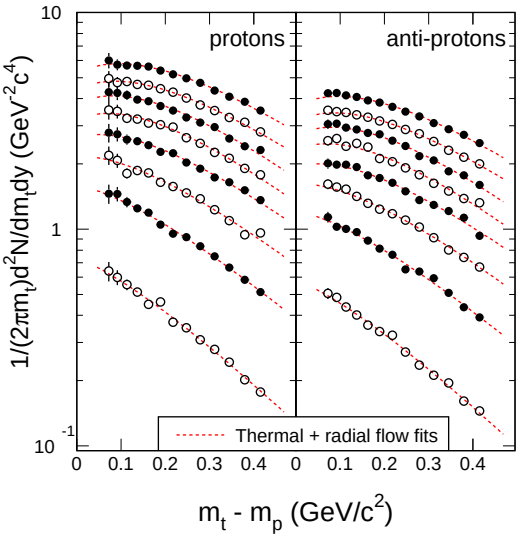

Figure 6 *Mid-rapidity ($|y| \leq 0.5$) proton (left column) and anti-proton (right column) transverse mass distributions for most peripheral (bottom) to most central (top) collisions. Relatively large systematic errors for protons in the low p_T region are due to background subtraction. The thermal model fit results are shown as dashed lines. This figure is taken from Ref. [31]*

Proton Results: The mid-rapidity ($|y| \leq 0.5$) proton and anti-proton transverse mass distributions are shown in Figure 6 for 8 centrality bins. These data are from $Au+Au$ collisions at 130 GeV [31]. Here, the transverse mass m_t is given by $m_t = \sqrt{(p_t^2 + m^2)}$, with m the rest mass of proton (anti-proton). It is evident that both proton (left panel) and anti-proton (right panel) distributions become more convex from peripheral to central collisions. This increase with centrality is also reflected in the values of $\langle p_t \rangle$, shown in Figure 7. In order to extract total yields, dN/dy and mean transverse momenta $\langle p_t \rangle$, thermal model fits [32] were applied. These fits simultaneously describe experimental spectra of charged pions [33], kaons [34], protons and anti-protons. The fit-results are shown as dashed lines in Figure 6. The velocity profile $\beta_t(r) = \beta_s(r/R)^{0.5}$ was used in the fits, where R and β_s are the radius and the surface velocity of the source, respectively. When strong collective flow develops, the transverse mass distributions for heavy mass particles

will not have a simple exponential shape at low transverse mass. This effect becomes particularly strong when the temperature is low. The hydrodynamically motivated two parameter fits (T_{fo}, β_t) then become necessary [35]. The increase of $\langle p_t \rangle$ with centrality is indeed reflected in the values of the collective velocity parameter $\langle \beta_t \rangle$, which increase from about $0.41c$ to $0.55c$ from the most peripheral to the most central collisions, respectively [31].

The top panels of Figure 7 show $\langle p_t \rangle$ within $|y| \leq 0.5$ for protons (left) and anti-protons (right). The corresponding yields, dN/dy are shown in the bottom panels. The open symbols represent fiducial yields and filled ones show the extrapolated total yields. The hatched bands indicate the systematic uncertainties in extracting $\langle p_t \rangle$ and dN/dy. The increase of $\langle p_t \rangle$ vs. centrality in the figure implies the development of stronger collective expansion in more central collisions. Results from calculations with RQMD [36], RQMD with re-scattering switched off, and HIJING [9,37] are represented by solid, dashed, and dashed-dotted lines, respectively. In the RQMD model [36,38] hadronic re-scattering has been implemented, which leads to the agreement with measurements of the mean transverse momentum. On the other hand, without the re-scattering mechanism, the HIJING model under-predicts the proton (anti-proton) $\langle p_t \rangle$, especially for central collisions. Overall, the model calculations fail to predict the experimental yields consistently throughout the whole centrality range.

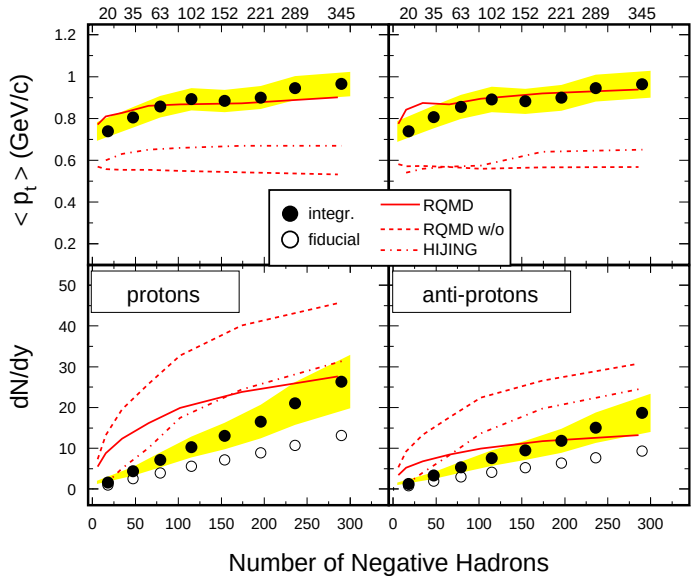

Figure 7 *Mid-rapidity $\langle p_t \rangle$ and dN/dy of proton and anti-proton as a function of the number of negatively charged hadrons. The data are from $Au + Au$ collisions at 130 GeV. Open symbols are fiducial yields and filled ones are total yields. Systematic errors in the integrated yields are shown as hatched areas. Results from RQMD with re-scattering switched off (w/o) and HIJING are shown as solid-lines, dashed-lines and dashed-dotted lines respectively. The experimental data and the results from RQMD and HIJING include feed-down from hyperon decay. The number of the participants for each centrality is also shown at the top of the plots. This figure is taken from Ref. [31]*

As one can see from the bottom panels of Figure 7, the observed mid-rapidity ($|y| \leq 0.5$)

proton and anti-proton yields, dN/dy are found to be proportional to the number of charged hadrons. RQMD fails to predict the centrality dependence of the anti-proton yield due to the strong annihilation in hadronic re-scattering, especially in central collisions. Because of the annihilation, RQMD predicts a change in the $\overline{p}/p$ ratio of almost a factor of two from peripheral to central collisions, which is not consistent with observations [39].

The results from RQMD show that late hadronic re-scatterings build up large values of $\langle p_t \rangle$ and lead to strong annihilation among baryons. In the RQMD calculations the annihilation of initially created anti-protons increases from 20% in peripheral collisions to 50% in the most central collisions. The experimental data exhibit an approximately linear increase in proton and anti-proton yields with the number of negatively charged hadrons (see Figure 7). We may therefore reach the following conclusions: On one hand, if the annihilation of baryons with anti-baryons increases with centrality, then the centrality dependence of the initial baryon production rate can only be stronger than linear as currently observed. Thus our experimental yields may be inconsistent with the initial baryon production mechanism in the RQMD model. On the other hand, if the initial baryon production is correctly modeled by RQMD, then our measurement indicates a smaller anti-proton loss due to annihilation in the most central collisions. In this case, protons and anti-protons might have inherited collective flow from an earlier stage [40,41] in order to attain the large experimental values of $\langle p_t \rangle$. In order to distinguish different scenarios and possible early stage partonic collectivity at RHIC, a systematic measurement of multi-strange baryons, charmed mesons and particle correlations becomes necessary.

Within STAR, the particle identification (PID) based on the TPC dE/dx information becomes very difficult at $p \sim 1$ GeV/c. Other methods like the mixed-event, decay-topology, photon-conversion are employed for PID in STAR. Due to the large acceptance and high efficiency of the STAR TPC, these methods are very effective and suffer very small edge effects [42]. In STAR, in addition to the measured stable particles, distributions of $\pi^0, K^0_S, K^*, \rho, \Delta^{\pm}, \phi, \Lambda, \Xi, \Omega, D^{0,\pm}, D^*$ have been measured [24,26,43–47].

In Figure 8, the mid-rapidity transverse momentum distributions (the invariant spectra are plotted as a function of $m_T -$ mass) for pions, Kaons, protons [50], ϕ [25], Λ, Ξ, and Ω [49,51], from $\sqrt{s_{\rm NN}} = 200$ GeV $Au+Au$ collisions, are shown. While pion spectra show a p_T-power-law shape, most of the hadron spectra are m_T-exponential, especially the strange hadrons like K, ϕ, Ξ and , Ω. In order to characterize the transverse motion, exponential fit[2] or a power-law fit[3] is often used for the measured spectra. In addition, for spectra extracted from heavy ion collisions, hydrodynamics motivated fits [32] are applied to the measured spectra.

---

[2] $$f_{exp} = A \cdot e^{-m_T/T},$$

where A and T are the normalization constant and inverse slope parameter, respectively.

[3] $$f_p = A \cdot (1 + \frac{p_T}{p_0})^{-n},$$

here A is the normalization constant and p_0 and n are free parameters that describe the shape of the distributions. In high-energy elementary collisions, mesons are following the power-law type while the baryons are more close to the exponential function [48].

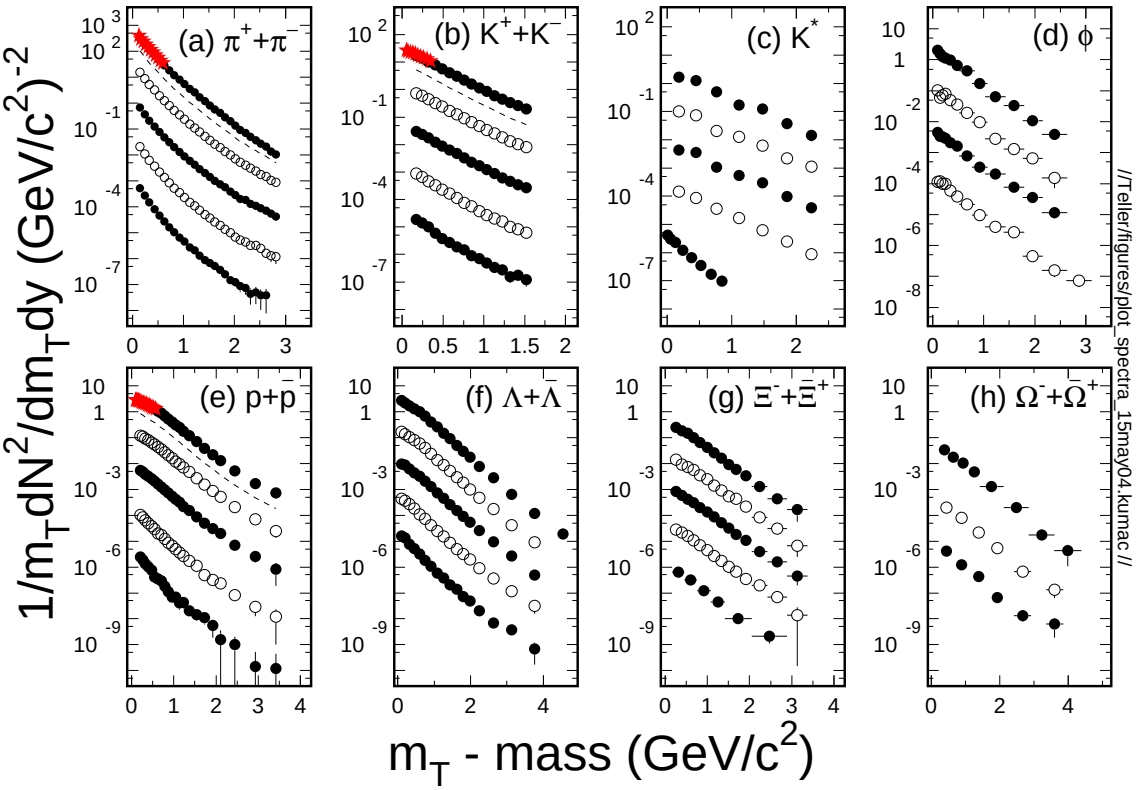

Figure 8 *Mid-rapidity hadron spectra from* $\sqrt{s_{\rm NN}}$ *= 200 GeV* $Au+Au$ *collisions. Most and least central collisions are listed from top-down. For pions (a), Kaons (b), and protons (e) [50], the centrality bins are: 0-5%, 20-30% (*10^{-1}*), 40-50% (*10^{-2}*), 60-70% (*10^{-3}*), and 80-92% (*10^{-4}*). The star symbols (0-5%) are data from [49]. In parenthesizes are the scaling factors and dashed-lines represent the spectra from minimum biased collisions. For* K^* *(c), from top to bottom, respectively, the centralities are 0-10%, 10-30%, 30-50%, 50-80% for* $Au+Au$ *collisions and* $p+p$ *collisions. For* ϕ*-meson (d) [25], the centralities are: 0-5%, 10-30% (*10^{-1}*), 30-50% (*10^{-2}*), and 50-80% (*10^{-3}*). For* Λ *(f) and* Ξ *(g) [51], the centrality bins are: 0-5%, 10-20% (*10^{-1}*), 20-40% (*10^{-2}*), 40-60% (*10^{-3}*), 60-80% (*10^{-4}*). For the* Ω *baryon (h) [51], the centralities are: 0-10%, 20-40% (*2×10^{-2}*), and 40-60% (*10^{-3}*).*

ϕ Results: As can be seen in Figure 8, all multi-strange hadron distributions fit well with an exponential function. In contrast to the distributions of π, K, and protons, the slope parameters of both ϕ, Ξ, and Ω show little sensitivity to the changing of collision centrality. As an example, the values of ϕ $\langle p_t \rangle$ are compared to that of π, K, and anti-proton [49], see Figure 9, plot (a). The general trend for $\bar{p}$, K^- and π^- is an increase in $\langle p_t \rangle$ as a function of centrality, which is indicative of an increased transverse radial flow velocity component to these particles' momentum distributions. The ϕ $\langle p_t \rangle$, however, increases from $p+p$ to $Au+Au$, but has no significant centrality dependence in $Au+Au$ collisions. This indicates that the ϕ does not participate in the transverse radial flow as do the $\bar{p}$, K^- and π^-. This is expected, however, if the ϕ decouples early in the collision before transverse radial flow has been completely built up. If the ϕ hadronic scattering cross section is much smaller than that of other hadrons, one would not expect the ϕ $\langle p_t \rangle$

distribution to be strongly affected by any final state hadronic rescatterings.

The yield ratio ϕ/K^- from this analysis is constant as a function of centrality as shown in Figure 9 (b) and beam energy Figure 9 (d). In fact, for collisions above the threshold for ϕ production, the ϕ/K^- ratio is essentially independent of system size, e^+e^- to nucleus-nucleus, and energy from a few GeV up to 200 GeV (Figure 9 (d)) [52–57]. This is remarkable, considering that the initial conditions of an e^+e^- collision are drastically different from $Au + Au$ collisions. This observation perhaps indicates that the ratio is dominated by the hadronization process.

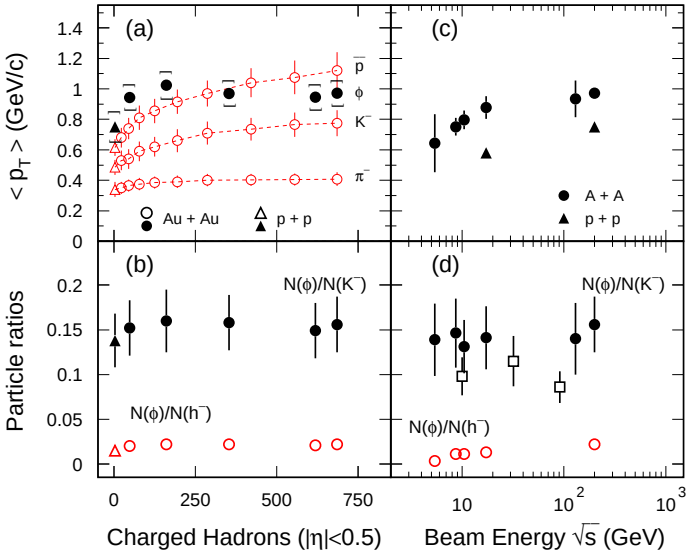

Figure 9 *(a) ϕ $\langle p_t \rangle$ vs. measured number of charged hadrons (N_{ch}) within $|\eta| \leq 0.5$. For comparison, the values of $\langle p_t \rangle$ for negative pions, kaons, and anti-protons are also shown; (b) Ratios of $N(\phi)/N(K^-)$, filled symbols, and $N(\phi)/N(h^-)$, open symbols, vs. N_{ch}; (c) $\langle p_t \rangle$ vs. center of mass beam energy from central nucleus-nucleus (filled circles) and $p + p$ collisions (filled triangles); (d) Ratios of $N(\phi)/N(K^-)$ from central nucleus nucleus collisions, filled circles, and $N(\phi)/N(h^-)$, open circles, vs. center of mass beam energy. Data from e^+e^- (open squares) are also shown. All plots are from mid-rapidity. Both the statistical and systematic errors are shown for the 200 GeV STAR data, while only statistical errors are shown for the energy dependence of the particle ratios.*

Rescattering models (RQMD[36], UrQMD[58]) assume that about 2/3 of ϕ mesons come from kaon coalescence in the final state. The centrality dependence of the ϕ/K^- ratio alone provides a serious test of the current rescattering models. In these models, rescattering channels for ϕ production includes $K\bar{K}$ and K-Hyperon modes. They predict an increasing ϕ/K^- ratio vs. centrality. These models also predict an increase in $\langle p_t \rangle$ for the proton, kaon, and ϕ of 40 to 50% from peripheral to central collisions. A comparison of the data to these models rules out the kaon coalescence production mechanism for ϕ mesons.

Freeze-out Properties: Figure 10 shows a qualitatively different behavior, in the temperature versus collective velocity plane, between the relatively rarely produced multi-strange particles and copiously produced particles π, K and protons. The χ^2 contours are ex-

tracted from the thermal + radial flow fits [32] and presented in the temperature-velocity space. The numerical labels indicate the centrality selection. For π, K and protons, 9 centrality bins were used from the 200 GeV $Au + Au$ collisions and $p + p$ collisions [49]. For ϕ and Ω, only the most central results are shown. Dashed- and solid-lines are the 1-σ and 2-σ contours, respectively.

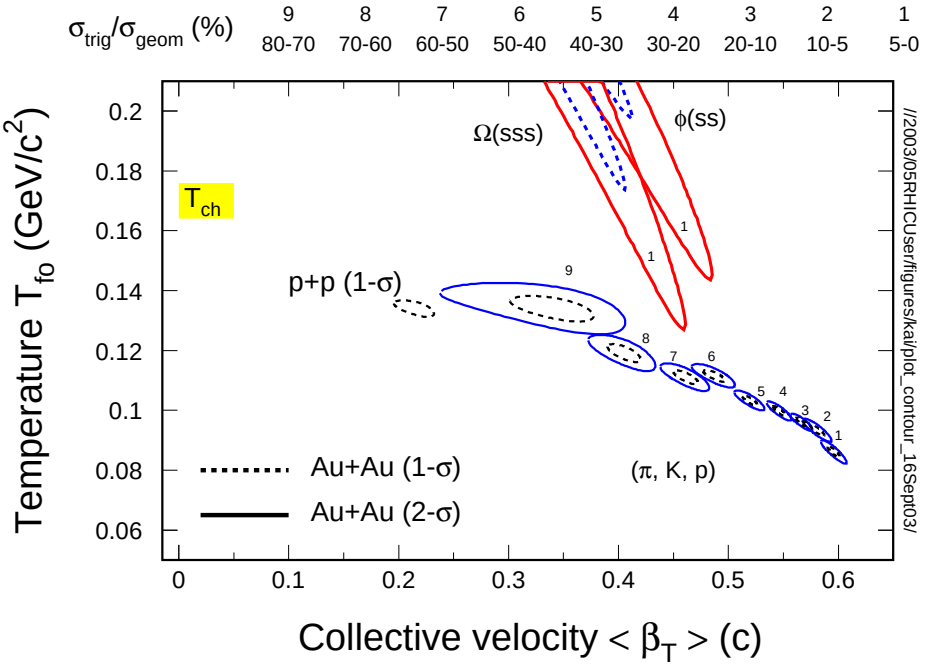

Figure 10 χ^2 *contours, extracted from the thermal+radial flow fits, for copiously produced hadrons* π, K *and protons and multi-strange hadrons* ϕ *and* Ω*. On the top of the plot, the numerical labels indicate the centrality selection. For* π, K *and protons, 9 centrality bins (from top 5% to 70-80%) were used from 200GeV* $Au + Au$ *collisions. The results from 200GeV* $p + p$ *collisions are also shown. For* ϕ *and* Ω*, only the most central results are presented. Dashed- and solid-lines are the 1-*σ *and 2-*σ *contours, respectively.*

As the collision centrality changes from peripheral to central, for copiously produced hadrons, π, K and protons, the temperature parameter decreases and the velocity parameter increases. At the most central collisions, the velocity becomes as high as 60% of the speed of light. On the other hand, the fit results indicate that the minima for multi-strange hadrons are not sensitive to collisions centrality and they are all close to a temperature of T $\sim$ 180 MeV and the average velocity of $\beta \sim 0.4c$.

While thermal freeze-out temperature for π, K and proton is about 100 MeV, the temperature parameter from the multi-strange hadrons is the same as the chemical freeze-out temperature [59–63] and it is close to the value of the phase transition temperature [2]. Due to relatively small total hadronic cross sections [64,65], multi-strange particles do not participate in the evolution of the system during the hadronic phase. As a result, they de-associate from the system near the hadronization point with $T \sim 170$ MeV and $\beta \sim 0.4c$

4. Elliptic flow v_2 – Evidence for partonic collectivity at RHIC

The particle azimuthal distribution with respect to the reaction plane at a given rapidity window can be deconvoluted by the expansion:

$$\frac{dN}{d\phi} \approx v_0(1 + 2v_1\ \cos(\Delta\phi) + 2\mathrm{v}_2\ \cos(2\Delta\phi)). \tag{3}$$

The first and second Fourier coefficients, v_1 and v_2, are connected to direct flow and elliptic flow, respectively. The coefficient v_0 is a normalization constant and $\Delta\phi$ is defined as the azimuthal angle difference between the particle and the event reaction plane. At a given rapidity the coefficients are: $v_1 = \langle\cos(\Delta\phi)\rangle$ and $v_2 = \langle\cos(2\Delta\phi)\rangle$, commonly noted as directed and elliptic flow, respectively. Because the rescattering induced expansion naturally reduces the spatial anisotropy, the early information of the collision dynamics can be learned through measuring v_1, v_2 and higher order harmonics [66–70].

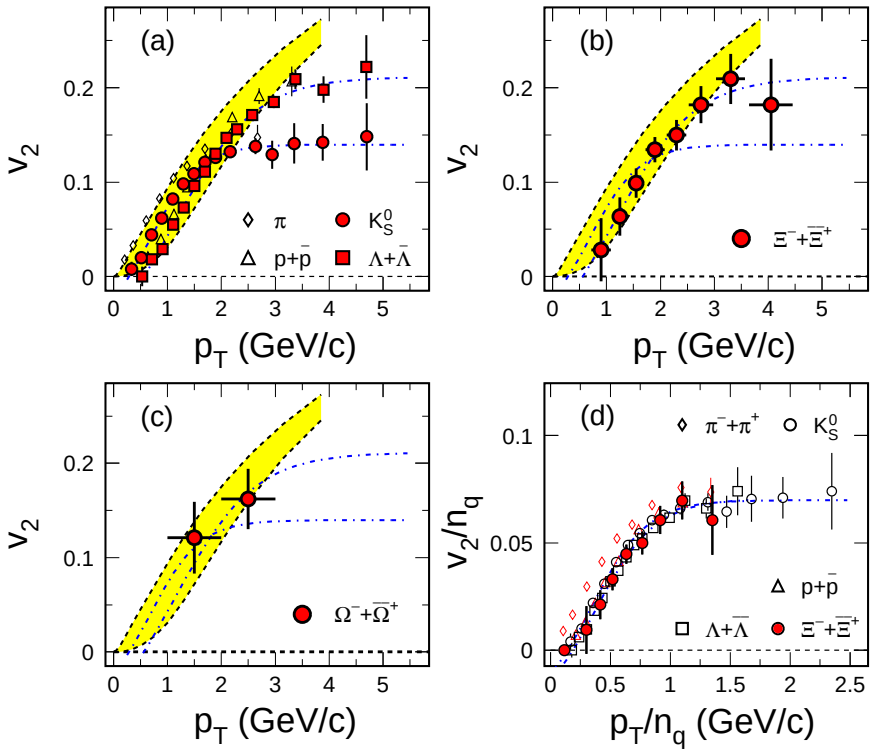

Figure 11 *(a) Experimental results of the transverse momentum dependence of the event anisotropy parameters for π, K^0_S, $p + \overline{p}$, $\Lambda + \overline{\Lambda}$. Dot-dashed lines are the results of fits. Hydrodynamic calculations are shown as thick-dashed-lines. From top-down are the results for π, K, p, Λ, $\Xi^- + \overline{\Xi}^+$, and $\Omega^- + \overline{\Omega}^+$; Multi-strange baryon elliptic flow v_2 are shown in (b) for Ξ and (c) for Ω.Plots (b) and (c) are from preliminary STAR results [51,71]. (d) Number of constituent quark (n_q) scaled v_2/n_q versus scaled p_T/n_q.*

The measured elliptic flow v_2 from the minimum bias $Au + Au$ collisions at $\sqrt{s_{\rm NN}} =$ 200 GeV for $\pi, K^S_0, p,\ \Lambda$ are shown in Figure 11 (a). The results of pions and protons are from the PHENIX experiment [72]. Respectively, from top to bottom the dashed-lines represent the elliptic flow of $\pi, K, p, \Lambda, \Xi, \Omega$ from hydrodynamic calculations [73]. At lower

p_T, the v_2 results are well reproduced by the hydrodynamic calculations. At higher p_T, v_2 becomes saturated and hydrodynamic results over-predict the data. While the baryons saturate at $p_T \geq 3$ GeV/c with $v_2 \sim 0.2$, mesons saturation starts earlier at lower values of v_2.

Figure 11 (b) and (c) show v_2 for the multi-strange baryons $\Xi^- + \overline{\Xi}^+$ and $\Omega^- + \overline{\Omega}^+$, respectively. Although they tend to suffer much less rescatterings in the hadronic stage of the collisions, see Figure 10, the values of v_2 for strange-baryons are found to be as high as other hadron at given p_T . Hence again the collectivity must be developed at the partonic stage.

The measured v_2 distributions are fitted with the equation given as;

$$f_{v_2} = \frac{a}{1 + exp(-(x-b)/c)} - d \tag{4}$$

where parameters a, b, c and d are fixed from the fit. The fit results to K^0_S and Λ are shown as dot-dashed lines in Figure 11 (a). According to coalescence approaches [74], after scaling both values of v_2 and p_T with the number of the constituent quarks (NCQ) of the corresponding hadron, all particles should fall onto one single curve. Figure 11 (d) shows the scaled v_2. Indeed all particles follow one curve except the pions. This means that there is collectivity developed at the partonic stage. In the NCQ scaled plot, Figure 11 (d), the fit results are also shown as dashed lines. For kaon, proton and lambda, the scaling seems to be working within $p_T/n_q \leq 2.5$ GeV/c. Pions (open triangles) do not follow the scaling, because of a large fraction of hadrons produced through resonance decays. This is particularly true for pions in high-energy heavy ion collisions [75,76]. At mid-rapidity, in collisions at RHIC, as high as $\sim 80\%$ of pions are from resonance decays and the dominant sources for pion production are ρ, ω and baryon resonances like Λ.

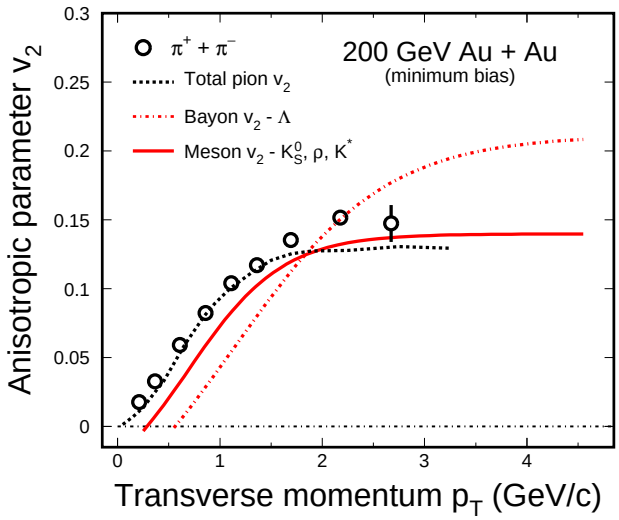

Figure 12 *Resonance decayed pion v_2 (symbols) versus transverse momentum. Dashed line represents the sum of the resonance decay effects. Solid and dot-dashed lines are the v_2 versus p_T curves for mesons and baryons, respectively.*

In order to test this idea, we need two basic pieces of information on the resonance production. First is their v_2 distributions. Assuming the NCQ-scaling, as demonstrated in Figure 11, one can readily estimate their v_2 distributions via Eq. (4). Secondly one needs to know the relative yields of the resonances. This information is determined from the chemical fits [63] provided the relative yields are fixed at chemical freeze-out.

The simulated result is shown as dashed line in Figure 12. Resonances of ρ, ω, K^*, K^0_S and Λ are used in this study [77]. The dominant resonance is the ρ-mesons. As one can see, when resonance decays are taken into account, the v_2 of primary pions becomes consistent with a NCQ-scaling. The observation of the NCQ-scaling, which can be a natural consequence of hadrons coalescing out of a thermal distribution of partons and the finite values of collective radial flow velocity parameter for multi-strange hadrons freeze-out at T_{ch} (see Figure 10), indicates that partonic flow develops at RHIC.

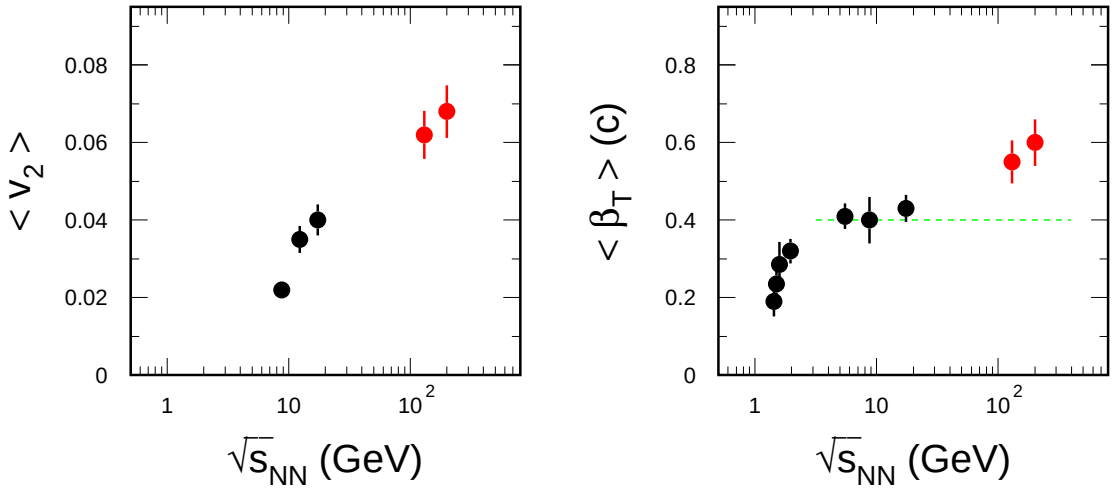

Figure 13 *Collision energy dependence of (Left) the elliptic flow v_2 from minimum biased $Au + Au$ or $Pb + Pb$ interactions; (Right) the radial flow velocity parameter $\langle\beta_T\rangle$ from central $Au + Au$ or $Pb + Pb$ collisions.*

Let us close this section by showing the collision energy dependence of the collective flow observables. In Figure 13, the elliptic flow v_2, and the radial flow parameters, β_T, are shown as a function of collision energy. The values of v_2 increase monotonically implying that more and more early collectivity develops as the collision energy increases (see left plot). Assuming that hadronic rescattering effects have already been maximized at SPS energies ($\sqrt{s_{\rm NN}} \approx 17$ GeV), the net increase in the transverse velocity at RHIC perhaps is due to partonic interactions (right plot).

5. Summary and outlook

In summary, the suppression of hadron production at intermediate transverse momentum region ($3 \leq p_T \leq 10$) in central $Au + Au$ and the results from the $d + Au$ collisions provide evidence of early stage, most likely partonic, interactions at RHIC. As a result, the bulk matter created at RHIC demonstrates a stronger collective expansion with larger

values of elliptic flow - the development of partonic collectivity. The NCQ-scaling behavior has been observed in both v_2 and R_{CP}, further confirms that the partonic collectivity is developed before hadronization, provided that the coalescence procedure took place over a volume that is much larger than the one created in any elementary collisions.

In the near future, it is important to quantify the partonic collective flow with high statistics data of v_2 measurements for all hadrons. The results of ϕ-meson v_2 and R_{AB} are especially important because ϕ-mesons are unlikely to be produced through kaon fusion [25]. These results will provide direct information on the partonic phase.

The next step, perhaps the last necessary measurement needed for the EOS measurement of partonic matter, *i.e.* QGP, is the proof of the thermalization for light quarks. According to up to date theoretical predictions, the QGP temperature is in the order of 0.3 - 0.5 GeV [78,79]. The mass of the charm-quark is much heavier than the possible temperature, meaning that thermal excitation of the charm-quark is negligible. Because of their heavy mass, the development of heavy flavor collectivity requires much more partonic rescatterings. Hence the measurement of heavy flavor [80] (open-charm for example) v_2 should be used to probe the equilibrium status of light quarks like u,d, and s at RHIC, in addition to the conventional methods of temperature measurements with thermal photons and di-leptons.

As mentioned in the introduction, the Lattice calculations predict both phase (hadronic to partonic) and chiral symmetry transitions occur simultaneously [1,2]. Therefore it is necessary to study the hadron properties experimentally. This is possible with the measurements of leptons in several experiments [81,82] at RHIC.

We are grateful for many enlightening discussions with Drs. P. Braun-Munzinger, C. Ko, M. Gyulassy, U. Heinz, P. Huovinen, F. Liu, A. Poskanzer, H.G. Ritter, K. Schweda, P. Sorensen, E.V. Shuryak, and Z. Xu. This work has been supported by the U.S. Department of Energy under Contract No. DE-AC03-76SF00098.

REFERENCES

1. H. Satz, Nucl. Phys. **A715**, 3c(2003).
2. F. Karsch, Nucl. Phys. **A698**, 199c(2002).
3. Z. Fodor, Nucl. Phys. **A715**, 319c(2003) and references there in; Z. Fodor and S.D. Katz, Phys. Lett. **B534**, 87(2002).
4. W. Reisdorf and H.G. Ritter, Ann. Rev. Nucl. Part. Sci. **47**, 663(1997).
5. C. Adler *et al.*, (STAR Collaboration), Phys. Rev. Lett. **89**, 202301(2002).
6. J. Adams *et al.*, (STAR Collaboration), Phys. Rev. Lett. **91**, 172302(2003).
7. C. Adler *et al.*, (STAR Collaboration), Phys. Rev. Lett. **90**, 082302(2003).
8. X.N. Wang and M. Gyulassy, Phys. Rev. Lett. **68**, 1480(1992).
9. X.N. Wang, Phys. Rep. **280**, 287(1997).
10. P.L. McGaughey, J.M. Moss, and J.C. Peng, Ann. Rev. Nucl. Part. Sci. **49**, 217(1999).
11. D.M. Alde *et al.*, Phys. Rev. Lett. **64**, 2479(1990).
12. M. Begel, Ph.D Thesis, Rochester University, 1999.
13. K. Adcox *et al.*, (PHENIX Collaboration), Phys. Rev. Lett. **88**, 022301(2002).
14. S.S. Adler *et al.*. (PHENIX Collaboration), Phys. Rev. **C69**, 034901(2004).

15. S.S. Adler *et al.*, (PHENIX Collaboration), Phys. Rev. Lett. **91**, 072301(2003).
16. C. Adler *et al.*, (STAR Collaboration), Phys. Rev. Lett. **90**, 032301(2003).
17. C. Adler *et al.*, (STAR Collaboration) Phys. Rev. Lett. **90**, 082302(2003).
18. D. Kharzeev, E. Levin, and L. McLerran, Phys. Lett. **B561**, 93(2003).
19. M. Gyulassy, I. Vitev, X.N. Wang, and B. Zhang, nucl-th/0302077 and references therein.
20. K. Gallmeister, C. Greiner, and Z. Xu, Phys. Rev. **C61**, 044905(2003).
21. S.S. Adler *et al.*, (PHENIX Collaboration), Phys. Rev. Lett. **91**, 072303(2003).
22. I Arsene *et al.*, (BRAHMS Collaboration), Phys. Rev. Lett. **91**, 072305(2003).
23. B.B. Back *et al.*, (PHOBOS Collaboration), Phys. Rev. Lett. **91**, 072302(2003).
24. J. Adams *et al.*, (STAR Collaboration), Phys. Rev. Lett. **92**, 052302(2004).
25. E. Yamamoto, (STAR Collaboration), Nucl. Phys. **A715**, 466c(2003).
26. J. Adams *et al.*, (STAR Collaboration), Phys. Rev. Lett. **92**, 182301(2004).
27. J.W. Cronin *et al.* Phys. Rev. Lett. **31**, 1426(1973); J.W. Cronin *et al.* Phys. Rev. **D11**, 3105(1975); D. Antreasyan *et al.* Phys. Rev. **D19**, 764(1979).
28. P.B. Straub *et al.*, Phys. Rev. Lett. **68**, 452(1992).
29. Enke Wang and Xin-Nian Wang, Phys. Rev. Lett. **87**, 142301(2001).
30. F.Q. Wang *et al.* (STAR Collaboration), J. Phys. G: Nucl. Part. Phys. **30**, S1299(2004).
31. J. Adams *et al.*, (STAR Collaboration), Phys. Rev. **C**, Rapid Communications, in print, (2004).
32. E. Schnedermann, J. Sollfrank, and U. Heinz, Phys. Rev. **C48**, 2462(1993).
33. J. Adams *et al.*, (STAR Collaboration), nucl-ex/0311017.
34. C. Adler *et al.*, (STAR Collaboration), Phys. Lett. **B**, in print, (2004).
35. I. G. Bearden *et al.*, (NA44 Collaboration), Phys. Rev. Lett **78**, 2080(1997); M. Kaneta, Ph.D Thesis, (NA44 Collaboration), March (1999).
36. H. Sorge, Phys. Rev. **C52**, 3291 (1992).
37. S.E. Vance, M. Gyulassy, and X.N. Wang, Phys. Lett. **B443**, 45(1998); S.E. Vance, Nucl. Phys. **A661**, 230c(1999).
38. B. Monreal *et al.*, Phys. Rev. **C60**, R31903(1999); *ibid.* Phys. Rev. **C60**, R51902(1999).
39. C. Adler *et al.*, (STAR Collaboration), Phys. Rev. Lett. **86**, 4778(2001); *ibid.* **87**, 262302(2001).
40. L. McLerran and J. Schaffner-Bielich, Phys. Lett. **B514**, 29(2001).
41. K.H. Ackermann *et al.*, (STAR Collaboration), Phys. Rev. Lett. **86**, 402(2001).
42. M. Anderson *et al.*, Nucl. Instrum. Meth. **A499**, 659(2003).
43. I.J. Johnson *et al.*, (STAR Collaboration), Nucl. Phys. **A715**, 691c(2003).
44. C. Adler *et al.*, (STAR Collaboration), Phys. Rev. Lett. **89**, 092301(2002).
45. C. Adler *et al.*, (STAR Collaboration), Phys. Rev. **C66**, 061901(R)(2002).
46. J. Adams *et al.*, (STAR Collaboration), Phys. Rev. Lett. **92**, 092301(2004).
47. Zhang-bu Xu, nucl-ex/0307014, (2003).
48. G. Bocquet *et al.* (UA1 Collaboration), Phys. Lett. **B366**, 441(1996).
49. J. Adams *et al.*, (STAR Collaboration), Phys. Rev. Lett. **92**, 112301(2004).
50. S.S. Adler *et al.*, (PHENIX Collaboration), Phys. Rev. **C69**, 034909(2004).
51. K. Schweda *et al.*, (STAR Collaboration), J. Phys. G: Nucl. Part. Phys., **30**,

S693(2004).
52. K. Hagiwara *et al.*, Phys. Rev. **D66**, 010001 (2002) and references within.
53. S.V. Afanasiev *et al.*, (NA49 Collaboration), Phys. Rev. **C66**, 054902 (2002).
54. B.B. Back *et al.*, (E917 Collaboration), Phys. Rev. **C69**, 054901(2004).
55. S.V. Afanasiev *et al.*, (NA49 Collaboration), Phys. Lett. **B491**, 59 (2000).
56. L. Ahle *et al.*, (E802 Collaboration), Phys. Rev. **C58**, 3523 (1998).
57. K. Adcox *et al.*, (PHENIX Collaboration), Phys. Rev. Lett. **88**, 242301(2002).
58. M. Bleicher *et al.*, J. Phys. G: Nucl Part. Phys. **25**, 1859-1896 (1999) and S. Bass *et al.*, Phys.Rev. **C60**, 021902(1999).
59. P. Braun-Munzinger, J. Stachel, J. Wessels, and N. Xu, Phys. Lett. **B344**, 43(1995); P. Braun-Munzinger, I. Heppe, and J. Stachel, Phys. Lett. **B465**, 15(1999).
60. F. Becattini, M. Gazdzicki, and J. Sollfrank, Eur. Phys. J. **C5**, 143(1998); F. Becattini, Z. Phys. **C69**, 485(1996); F. Becattini and U. Heinz, Z. Phys. **C76**, 269(1997).
61. J. Cleymans and K. Redlich, Phys. Rev. Lett. **81**, 5284(1998).
62. J. Letessier, J. Rafelski, and A. Tounsi, Phys. Lett. **B328**, 499(1994); M. Kaneta *et al.*, (NA44 Collaboration), J. Phys. G: Nucl. Part. Phys. **23**, 1865(1997).
63. N. Xu and K. Masashi, Nucl. Phys. **A698**, 306c(2001).
64. H. van Hecke, H. Sorge, and N. Xu, Phys. Rev. Lett., **81**, 5764(1998).
65. Y. Cheng, F. Liu, Z. Liu, K. Schweda, and N. Xu, Phys. Rev. **C68**, 034901(2003).
66. H. Sorge, Phys. Lett. **B402**, 251(1997).
67. J.-Y. Ollitrault, Phys. Rev. **D46**, 229(1992).
68. S. Voloshin, Nucl. Phys. **A715**, 379c(2003).
69. J. Adams *et al.*, (STAR Collaboration) Phys. Rev. Lett., **92**, 062301(2004).
70. N. Xu and Z. Xu, Nucl. Phys. **A715**, 587c(2003).
71. J. Castillo *et al.*, (STAR Collaboration), J. Phys. G: Nucl. Part. Phys., **30**, S1207(2004).
72. S.S. Adler *et al.*, (PHENIX Collaboration), Phys. Rev. Lett. **91**, 182301(2003).
73. P. Huovinen, P. Kolb, U. Heinz, P.V. Ruuskanen, and S. Voloshin, Phys. Lett. **B503**, 58(2001).
74. Z. Lin and C. Ko, Phys. Rev. Lett. **89**, 202302(2002); R.J. Fries, B. Mueller, C. Nonaka, S.A. Bass, Phys. Rev. Lett. **90**, 202303(2003); D. Molnar and S. Voloshin, Phys. Rev. Lett. **91**, 092301(2003).
75. Zhang-bu Xu, nucl-ex/0307014, (2003).
76. R.J. Fries, B. Mueller, C. Nonaka, S.A. Bass, Phys. Rev. **C68** 044902(2003); C. Nonaka,B. Mueller,M. Asakawa, S.A. Bass, and R.J. Fries, Phys. Rev. **C69**, 031902(2004).
77. X. Dong, S. Esumi, P. Sorensen, N. Xu, and Z. Xu, Phys. Lett. **B597**, 328(2004); V. Greco and C. Ko, Phys. Rev. **C70**, 024901(2004).
78. Edward V. Shuryak, Phys. Lett. **B78**, 150(1978).
79. R. Rapp, Phys. Rev. **C63**, 054907(2001).
80. E.L. Bratkovskaya, W. Cassing, H. Stoecker, and N. Xu, nucl-th/0409047 and references therein.
81. The PHENIX Collaboration, http://www.phenix.bnl.gov.
82. The STAR Collaboration, http://www.star.bnl.gov.